Field PMU Test and Calibration Method – Part I: General Framework and Algorithms for PMU Calibrator

Sudi Xu, Hao Liu, and Tianshu Bi

Abstract—Laboratory testing of phasor measurement units (PMUs) guarantees their performance under laboratory conditions. However, many factors may cause PMU measurement problems in actual power systems, resulting in the malfunction of PMU-based applications. Therefore, field PMUs need to be tested and calibrated to ensure their performance and data quality. In this paper (Part I), a general framework for the field PMU test and calibration in different scenarios is proposed. This framework consists of a PMU calibrator and an analysis center, where the PMU calibrator provides the reference values for PMU error analysis. Two steps are implemented to ensure the calibrator accuracy for complex field signals: ① by analyzing the frequency-domain probability distribution of random noise, a Fourier-transform-based signal denoising method is proposed to improve the anti-interference capability of the PMU calibrator; and 2 a general synchrophasor estimation method based on complex bandpass filters is presented for accurate synchrophasor estimations in multiple scenarios. Simulation and experimental test results demonstrate that the PMU calibrator has a higher accuracy than that of other calibrator algorithms and is suitable for field PMU test. The analysis center for evaluating the performance of field PMUs and the applications of the proposed field PMU test system are provided in detail in Part II of the next-step research.

Index Terms—Phasor measurement unit (PMU), calibration, synchrophasor, signal denoising, field PMU test.

I. INTRODUCTION

PHASOR measurement units (PMUs) can monitor the dynamic behavior of power systems in real time. Thus, they have been widely deployed in power systems [1]. The measurement performance and data quality of PMUs must be evaluated to ensure the reliability and effectiveness of wide-area measurement applications, i. e., state estimation [2], fault location [3] - [5], and out-of-step protection [6].

Manuscript received: August 2, 2021; revised: November 18, 2021; accepted: March 28, 2022. Date of CrossCheck: March 28, 2022. Date of online publication: June 27, 2022.

DOI: 10.35833/MPCE.2021.000526

Therefore, it is necessary to perform laboratory tests on PMUs before the installation [7].

However, laboratory tests alone do not guarantee the data quality of field PMUs for the following reasons: ① field power signals are more complex than test signals in a laboratory, e.g., dynamic fundamental signals, harmonics, interharmonics, and random noise may exist simultaneously [8]; (2) the hardware performance, i. e., the sampling module and synchronization module performances of field PMUs may decrease after long-term operation, and they need to be calibrated; and 3 older PMUs are not tested for compliance with new PMU standards. Therefore, field PMUs may have poor data quality, potentially reducing the stability of power systems. For example, incorrect measurements under offnominal conditions have resulted in false alarms consisting of low-frequency oscillation [9]. To this end, it is necessary to develop test methods for field PMUs to improve their measurement performance and data quality.

PMU test systems based on a high-precision generator (system GEN) or high-accuracy calibrator (system CAL) are commonly used to test the performance of PMUs. In system GEN [10] - [12], a high-precision generator sends standard test signals to the PMU under test (PUT), and the reference values are obtained according to the signal models of PMU standards. Subsequently, the measurements of the PUT are compared with the reference values to determine their performance. In system CAL [13]-[15], a generator simultaneously sends the test signals to the PUT and calibrator. The measurement results of the calibrator consider the reference values to obtain the performance of the PUT. In this test system, the generator does not require a high precision, but the accuracy of the calibrator must be at least 10 times higher than the standard requirements.

The literature indicates that three scenarios have been used to test field PMUs using the above two test systems, as shown in Fig. 1.

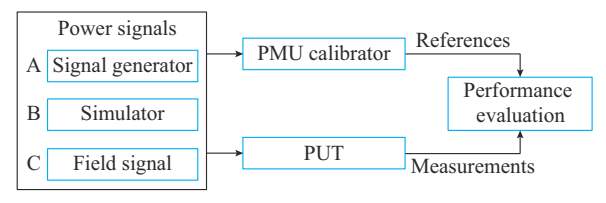


Fig. 1. Test system for field PMUs based on system CAL.



This work was supported by the National Natural Science Foundation of China (No. 51725702).

This article is distributed under the terms of the Creative Commons Attribution 4.0 International License (http://creativecommons.org/licenses/by/4.0/).

S. Xu, H. Liu (corresponding author), and T. Bi are with the State Key Lab of Alternate Electric Power System with Renewable Energy Sources (North China Electric Power University), Beijing, China, and S. Xu is also with the State Grid Jiangsu Electric Power Co., Ltd. Research Institute, Nanjing, China (email: 18515422011@163.com; hliu@ncepu.edu.cn; tsbi@ncepu.edu.cn).

In scenario A, the field PUT is disconnected from the power system, and a signal generator and a PMU calibrator are used to test the PMU, which is similar to laboratory test [16], [17]. The signal generator sends the test signals according to the PMU standards. It is determined whether the performance of the PUT satisfies the standard requirements under static and dynamic conditions. In this scenario, the reference values can be obtained according to signal models if the signal generator has a high output accuracy and timing accuracy. A PMU calibrator is not required.

Standard signals do not adequately represent the complex power signals. Thus, in scenario B, a signal generator or simulator is used for the playback simulation or field-recorded waveforms in various disturbance or fault scenarios [18]. In this case, the signal models are not known. Thus, a PMU calibrator is required to provide the reference values.

The above two test methods do not accurately represent the field signals. Additionally, the field PUT must be disconnected from the power system. Therefore, the PMU cannot monitor the system during the test. In scenario C, the PMU calibrator is connected to the power system to test the performance of the field PUT for field signals [19], [20]. However, the current line of the PUT and PMU calibrator must be connected in series. Thus, the PUT must be disconnected during the test. Noncontact measurement can be used to avoid line disconnection [19], but it is challenging to ensure the accuracy of noncontact current measurements. Therefore, the performance of the field PMU for voltage estimation is the focus of this test scenario.

System GEN is only suitable for scenario A, but system CAL can be used in all scenarios. Thus, a PMU calibrator can be used to test the field PMUs. The test signals in scenario A have known models. Thus, the calibrator algorithm can adjust the parameter setting according to the specific signal type [13]. The calibrator algorithm in scenarios B and C must be universal for complex power signals owing to the unknown signal models. The standard signals have low-noise levels, but the playback and field signals may have highnoise levels. Thus, the PMU calibrator requires good antinoise capability in scenarios B and C. In addition, the PMU calibrator in scenarios A and B has no real-time requirement, but that in scenario C needs to estimate the synchrophasor in real time. Therefore, different test scenarios have different requirements. It is valuable to develop a general test system framework of field PMUs to apply for multiple test scenari-

In system CAL, the synchrophasor algorithm of the calibrator is the key to providing a reference value with a sufficient accuracy in scenarios A, B, and C. However, the unknown test signal model and the high-noise level during the field PMU test in scenarios B and C make it difficult to calculate the reference values, which are the two problems that need to be solved in this paper.

Existing synchrophasor algorithms can be divided into PMU and calibrator synchrophasor algorithms. PMU synchrophasor algorithms can be categorized as time- and frequency-domain algorithms. Time-domain algorithms solve for the signal parameters iteratively and have numerical in-

stability [21], [22]. Thus, they are not suitable for the PMU calibrator in scenario C. Frequency-domain algorithms include discrete Fourier transform (DFT) based and Taylor Fourier transform (TFT) based algorithms. The DFT-based algorithms are based on the static synchrophasor model and have a low dynamic measurement accuracy [23], [24]. The TFT-based algorithms are based on the dynamic synchrophasor model and have better dynamic performance [25], [26]. However, TFT-based algorithms have a low synchrophasor accuracy for field signals with a large oscillation frequency, e.g., subsynchronous oscillation (SSO) of 30 Hz. Therefore, the frequency-domain algorithms do not meet the calibration requirements.

Existing calibrator algorithms have been proposed for the laboratory test of PMUs [13]-[15], [27]. In a typical algorithm, different fitting models are established according to the signal models in the PMU standards because the test type is known in the laboratory [13]. However, the signal models are unknown in scenarios B and C. Thus, these methods are not applicable. Therefore, universal methods are proposed such as the adaptive synchrophasor method, general fitting method, and frequency dynamic model method [18], [27]. These methods do not require prior information about the signal models. However, these methods have a poor antinoise capability for field signals and a low-measurement accuracy in the presence of high-frequency oscillation. These calibrator algorithms are not suitable for field PMU test in multiple scenarios. As a result, it is necessary to propose a high-accuracy synchrophasor algorithm for the field PMU

Most synchrophasor algorithms can filter the out-of-band (OOB) interference signals including random noise. However, the random noise in the measurement band is difficult to suppress, yielding a low-measurement accuracy. Therefore, a signal denoising method must be proposed to suppress the random noise in the measurement band. In addition, the PMU calibrator needs to estimate the synchrophasor in real time. Therefore, the denoising method must have a low computational complexity.

Signal denoising methods mainly include the digital filter method, adaptive filtering denoising [28], wavelet threshold denoising [29], empirical mode decomposition (EMD) [30], singular value decomposition (SVD) [31], Kalman filtering [32], and modern filtering theory such as Wiener filtering [33]. The digital filter method, e.g., EMD and SVD, removes the random noise outside the effective frequency band. However, they have poor denoising capability when the random noise overlaps the effective frequency band such as the dynamic fundamental signal. In addition, EMD and SVD cannot operate in real time because of their high computational complexities. The adaptive filtering method, modern filtering methods, and Kalman filtering method require prior knowledge of the field signal and noise. Therefore, they are not suitable for denoising-field power signals. Wavelet threshold denoising is essentially a low-pass filter, which cannot filter the noise in the low-frequency band, i.e., the measurement band of the PMUs. Therefore, the existing denoising methods have the problems of a high-calculation complexity or poor noise suppression in the frequency band for PMU measurement. A novel denoising method needs to be developed for field PMU test, especially for noisy dynamic power signals.

To address these problems, a field PMU test method is proposed, which is divided into Part I and Part II. The main contributions of Part I are as follows.

- 1) A general test and calibration framework consisting of a PMU calibrator and analysis center is proposed, which is the basis of the research work of Part I and Part II [34]. It is applicable to multiple test scenarios of field PMUs compared with other PMU test systems. The PMU calibrator is discussed in this paper, and the analysis center is analyzed in detail in Part II.
- 2) A high-accuracy synchrophasor estimation algorithm based on a complex bandpass filter is designed for the PMU calibrator. This algorithm is unrelated to the signal model and has good dynamic measurement performance for complex field signals.
- 3) According to the filtering characteristics of the synchrophasor algorithm, a Fourier-transform-based threshold denoising method is proposed, and an iterative threshold setting method based on a chi-squared distribution for the random noise is proposed. This method can further improve the accuracy of the PMU calibrator by eliminating the noise within the PMU measurement band.

The remainder of this paper is organized as follows. Section II presents a general test framework for field PMUs. In Section III, a synchrophasor estimation method is presented. A signal denoising method is proposed in Section IV. In Section V, the performance of the synchrophasor algorithm and denoising method is verified. Section VI summarizes this paper.

II. TEST FRAMEWORK FOR FIELD PMUS

According to the above analysis, a general test framework for field PMUs needs to have the following requirements. First, it can be applied to field PMU test for standard signals, playback signals, and field signals. Second, the PMU calibrator must have a high accuracy to provide the reference measurements, especially for noisy and dynamic field signals. Thus, the calibrator should provide good noise suppression to ensure its accuracy. Next, the fundamental signal type affects the performance evaluation of the PUT [7]. In scenarios A and B, the standard and playback signals have known signal types, or the types can be determined offline. However, the field signal types are unknown in scenario C. Thus, they must be determined in real time. Finally, the measurement performance of a field PMU is different at different interference levels, e.g., harmonics and interharmonics, leading to different evaluation indicators at different interference levels. Thus, it is necessary to calculate the content of the interference.

Consequently, the general framework for field PMU test is shown in Fig. 2, which consists of a PMU calibrator and an analysis center.

The PMU calibrator is used to provide reference values to analyze the estimation performance of the field PMUs. It in-

cludes five modules. The synchronous sampling module generates sampling clocks synchronized with the global positioning system (GPS) or Beidou and converts the voltage and current signals into sample values. The signal denoising module suppresses the random noise to improve the accuracy of the synchrophasor because the field signals may have highnoise levels, significantly affecting the accuracy of the synchrophasor. Then, the synchrophasor estimation module accurately measures the synchrophasor, frequency, and the rate of change of frequency (ROCOF) of the denoised power signals. In addition, the interference content module calculates the level of the interference signals to provide a reference for evaluating the performance of the PUTs. Simultaneously, a waveform recording module is used to record the power signals. Owing to the unknown models of complex field signals, it is difficult to determine the reason for the large test errors of the field PMUs. In this case, the recorded data can be used to ascertain which complex field signals have large errors.

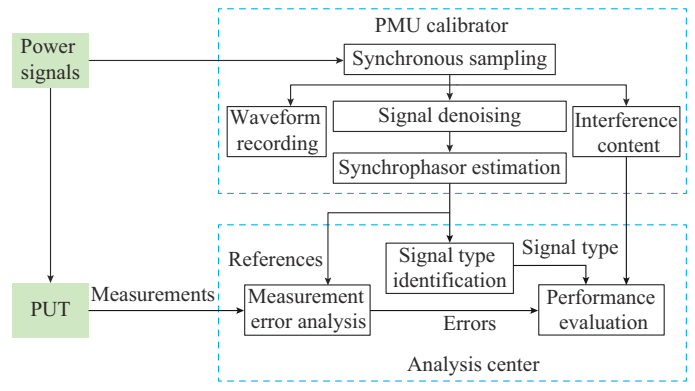


Fig. 2. General framework for field PMU test.

The analysis center is a computer that receives the measurement results and evaluates the performance of the field PMU, which includes three modules. First, the signal type identification module uses the synchrophasor measurements to identify the signal types such as the amplitude step and low-frequency oscillation because the field PMU has different measurement performances for different signal types. In addition, power systems are becoming increasingly complex because of the rapid development of renewables, flexible transmission, and active loads. Accordingly, the number of signal types may increase. Thus, this module must be gradually expanded and improved with the ongoing development of power systems.

Then, the measurement error analysis module obtains the measurement errors of the PUT by comparing the estimation results of the PMU calibrator and the PUT. The measurement errors include the total vector error (TVE), amplitude error (AE), phase error (PE), frequency error (FE), and RO-COF error (RFE). Finally, the performance evaluation module determines the error levels according to the signal types and interference levels because different signal types and interference levels have different error requirements. If there are doubts about the test results, the recorded data can be extracted for further analysis. In addition, this module gener-

ates test reports and allows the visualization of the test results.

It should be noted that not all the test scenarios require all these modules. For example, the signal models are known in scenario A. Thus, the signal type identification module and interference content module are not required. In other words, the proposed test framework can be simplified for various test scenarios.

The research works of Part I and Part II are carried out using this test framework. The PMU calibrator is the focus of Part I, and the analysis center is detailed in Part II. The synchronous sampling, waveform recording, and interference content modules are easily implemented [9], [14]. In contrast, the synchrophasor estimation and signal denoising modules of the PMU calibrator are the focus of the research work presented in this paper.

III. SYNCHROPHASOR ESTIMATION METHOD

The proposed synchrophasor algorithm for the PMU calibrator is based on the design method developed by our team [35]. However, different scenarios are utilized in this method. The application scenario of this paper is the field PMU test and calibration, and those in [35] are P- and M-class PMUs.

Static and dynamic signals can be regarded as a superposition of different frequency components. Therefore, a synchrophasor estimation method based on a complex bandpass filter is applied to measure the synchrophasor.

Generally, the field signals are not always in a static static, and their amplitudes and frequencies change slowly. The amplitude and frequency may significantly change under dynamic conditions such as those during low-frequency oscillation or SSO. Therefore, the power signal model can be expressed as:

$$v(t) = x(t) + \eta(t) = \sqrt{2} \ a(t)\cos(\varphi(t)) + \eta(t) \tag{1}$$

where x(t) is the fundamental signal; a(t) and $\varphi(t)$ are the time-varying amplitude and phase, respectively; and $\eta(t)$ is the interference signals, e.g., harmonics and OOB interharmonics.

According to the Euler formula, the fundamental signal can be divided into a positive frequency component and a negative frequency component as:

$$x(t) = \frac{\sqrt{2}}{2} a(t) \left(e^{j\varphi(t)} + e^{-j\varphi(t)} \right) = \frac{\sqrt{2}}{2} \left(X^{+}(t) + X^{-}(t) \right)$$
 (2)

where $X^+(t)$ and $X^-(t)$ are the positive and negative fundamental components, respectively.

Other interference signals can also be decomposed into symmetric components in the frequency domain. The diagram of the synchrophasor estimation method based on complex bandpass filters is shown in Fig. 3, where f_s is the sampling frequency; F_r is the reporting rate; and f_n is the nominal frequency.

The static and dynamic synchrophasors can be regarded as narrow-band components near the fundamental frequency (called the measurement bandwidth). Therefore, the synchrophasor can be obtained by extracting the positive fundamental component and suppressing the negative fundamental component using a complex bandpass filter. The field power signal must have harmonics and interharmonics. Therefore, the complex bandpass filter must filter the OOB interference components.

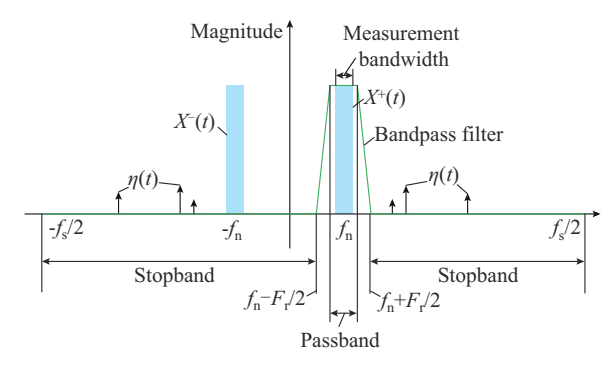


Fig. 3. Synchrophasor estimation method based on complex bandpass filters.

Filter design methods are mature. However, the challenge is to determine the parameter range of a complex bandpass filter for different scenarios. To this end, mathematical error models are derived to establish the relationship between the application requirements and the filter gain. Subsequently, the passband and stopband gains can be obtained using these models. The error models for the static and dynamic signals are described in [35]. The calibrator accuracy must be at least 10 times higher than the standard requirements. Based on the calibration requirements, the parameter range of the filter is obtained according to the error models. As shown in Table I, the passband ripple must be less than 0.0006 dB, and the stopband gain must be less than –95 dB for harmonics or OOB interharmonics and less than –129 dB for the negative fundamental component.

TABLE I

MEASUREMENT REQUIREMENTS AND PARAMETER RANGES OF FILTER FOR
PHASOR ESTIMATION METHODS FOR FIELD PMU TEST

Parameter	Range
Passband range (Hz)	45-55
Stopband range (Hz)	\leq 25 and \geq 75
Required passband ripple (dB)	< 0.0006
Designed passband ripple (dB)	0.0001
Required passband ripple of $X^{-}(t)$ (dB)	<-129
Designed passband ripple of $X^{-}(t)$ (dB)	-140
Required passband ripple of harmonic/OOB (dB)	<-95
Designed passband ripple of harmonic/OOB (dB)	-100
Data window (cycles)	15

Based on the "required" parameter range, the complex bandpass filter used for synchrophasor estimation is presented in Fig. 4. The passband ripple is less than 0.0001 dB, indicating that a positive fundamental component can be extracted accurately. The gain in the range of –55 Hz to –45 Hz is less than –140 dB, and the gain in the other stopband is

less than -100 dB. These parameter ranges are denoted as "designed" in Table I. Therefore, the negative fundamental component and OOB interference components can be suppressed effectively.

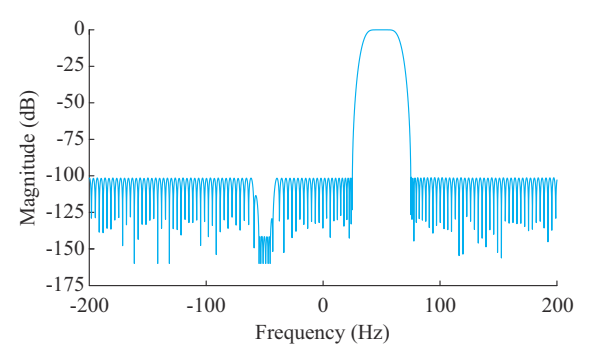


Fig. 4. Magnitude of response of calibrator synchrophasor algorithm for a reporting rate of 50 Hz.

Let the coefficients of the finite impulse response (FIR) bandpass filter in Fig. 4 be h(k) ($0 \le k \le 2M$, where 2M is the order of the filter). Then, the positive fundamental component can be obtained by:

$$z(k) = \sum_{i=0}^{2M} h(k)y(k - M + i)$$
 (3)

where y(k) is the discrete power signal; and z(k) is the measured positive fundamental component. The timestamp is marked in the middle of the data window to eliminate the phase shift.

Then, the synchrophasor at the reporting time can be obtained according to the definition of the synchrophasor:

$$\dot{X}(k) = \mathbf{z}(k)e^{-j2\pi f_n t_k} \tag{4}$$

where $\dot{X}(k)$ is the discrete synchrophasor; and t_k is the reporting time.

A high-accuracy measurement method for estimating the frequency and ROCOF is proposed in [9], and the details are presented in Appendix A. On the basis of these algorithms, the PMU calibrator provides an accurate synchrophasor, frequency, and ROCOF.

IV. SIGNAL DENOISING METHOD

A. Denoising Theory

A Fourier-transform-based threshold denoising method is proposed in this subsection. The detailed process is as follows.

The spectral coefficients Y(k) of the power signals are obtained by a DFT:

$$Y(k) = \sum_{n=0}^{M-1} y(n) e^{-j\frac{2\pi kn}{M}} \quad 0 \le k \le M - 1$$
 (5)

where M is the number of sampling values in the data window.

The spectral coefficients of the frequency components are larger than those of the random noise. Therefore, a threshold value is set to distinguish the significant components from noise:

$$Y'(k) = \begin{cases} Y(k) & Y(k) \ge S_{th} \\ 0 & Y(k) < S_{th} \end{cases}$$
 (6)

where S_{th} is the threshold value; and Y(k)=|Y(k)| is the amplitude. The spectral coefficients smaller than S_{th} are set to be 0, and the spectral coefficients greater than S_{th} remain unchanged.

The signal is reconstructed based on inverse DFT (IDFT) by using the new spectral coefficients:

$$y'(n) = real\left(\frac{1}{M} \sum_{k=0}^{M-1} Y'(k) e^{j\frac{2\pi kn}{M}}\right)$$
 (7)

where $real(\cdot)$ means the real part of a complex number.

The DFT and IDFT can be replaced by a fast Fourier transform (FFT) and an inverse FFT (IFFT), respectively, to reduce the computational burden. The key difficulty of the proposed denoising method is setting the threshold value, which is analyzed in detail later.

B. Random Noise Distribution

The random noise distribution in the frequency domain is first analyzed to determine S_{th} .

It is assumed that the random noise in power signals follows a normal distribution:

$$v(k) \sim N(\mu, \sigma^2) \quad 0 \le k \le M - 1 \tag{8}$$

where v(k) is the noise sequence; and μ and σ are the mean and standard deviations of the normal distribution, respectively. In general, μ is set to be 0. Thus, the noise is white Gaussian noise.

The DFT spectrum of the noise sequence is a complex sequence that can be expressed as:

$$V_{v}(k) = R_{v}(k) + jI_{v}(k)$$
 (9)

where $V_{\nu}(k)$ is the noise spectrum; and $R_{\nu}(k)$ and $I_{\nu}(k)$ are the real and imaginary parts of the noise spectrum, respectively.

The Fourier transform of a normal distribution also follows a normal distribution, and the real and imaginary parts have the same mean and standard deviations. Thus, we can obtain:

$$\begin{cases} R_{v}(k) \sim N(0, \sigma_{R}^{2}) \\ I_{v}(k) \sim N(0, \sigma_{I}^{2}) \end{cases} \quad \sigma_{V}^{2} = \sigma_{R}^{2} = \sigma_{I}^{2}$$
 (10)

where σ_R and σ_I are the standard deviations of the real and imaginary parts, respectively; and σ_V is the standard deviation of the noise spectrum.

The power and amplitude spectra of the white Gaussian noise are:

$$\begin{cases} P_{\nu}(k) = R_{\nu}(k)^{2} + I_{\nu}(k)^{2} \\ X_{\nu}(k) = \sqrt{P_{\nu}(k)} \end{cases}$$
 (11)

where $P_{\nu}(k)$ and $X_{\nu}(k)$ are the power and amplitude of the random noise, respectively.

The square sum of the random variables with a standard normal distribution has a chi-squared distribution. The number of degrees of freedom of the chi-squared distribution is equal to the number of random variables [36]. Based on this property, if the real and imaginary parts are standardized to follow a normal distribution in (12) and (13), the standardized power must obey the chi-squared distribution in (14).

$$R'_{\nu}(k) = \frac{R_{\nu}(k)}{\sigma_{\nu}} \sim N(0, 1)$$
 (12)

$$I_{\nu}'(k) = \frac{I_{\nu}(k)}{\sigma_{\nu}} \sim N(0, 1)$$
 (13)

$$P'_{\nu}(k) = (R'_{\nu}(k))^{2} + (I'_{\nu}(k))^{2} = \frac{P_{\nu}(k)}{\sigma_{V}^{2}} \quad P'_{\nu}(k) \sim \chi_{2}^{2}$$
 (14)

where $R'_{\nu}(k)$, $I'_{\nu}(k)$, and $P'_{\nu}(k)$ are the standardized real part, imaginary part, and noise power, respectively; and χ^2 is a chi-squared distribution with two degrees of freedom, whose probability density function is defined as:

$$g_n(x) = \begin{cases} \frac{1}{2^{n/2} \Gamma(n/2)} x^{n/2 - 1} e^{-x/2} & x > 0\\ 0 & x \le 0 \end{cases}$$
 (15)

where $\Gamma(\cdot)$ is the Gamma function; and n is the number of degrees of freedom (n=2 in this study). The probability of the chi-squared distribution is determined by its degrees of freedom.

C. Method of Threshold Setting

1) Threshold Characteristics

If the power spectrum of the random noise in the power signals can be obtained, it must have a chi-squared distribution after standardization according to the above analysis.

It is assumed that the power signal is as follows, and the signal-to-noise ratio (SNR) is 30 dB to 80 dB.

$$y(k) = x(k) + v(k) = 100\sqrt{2}\cos\left(2\pi \times 50.23\frac{k}{f_s}\right) + 20\sqrt{2}\cos\left(2\pi \times 27.47\frac{k}{f_s}\right) + 10\sqrt{2}\cos\left(2\pi \times 56.7\frac{k}{f}\right) + v(k)$$
(16)

The SNR is defined as:

$$SNR = 10 \lg \left(\frac{\sum_{k=0}^{M-1} x^2(k)}{\sum_{k=0}^{M-1} v^2(k)} \right)$$
 (17)

The probability density curves of chi-squared distribution χ_2^2 , random noise of 30 dB to 80 dB, and a noisy signal are shown in Fig. 5.

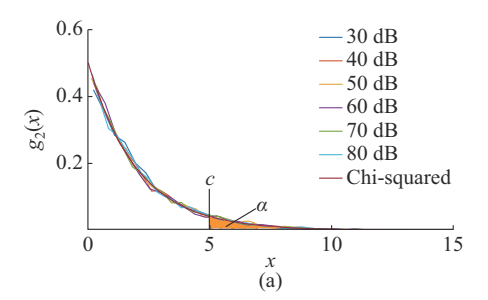
In Fig. 5(a), the random noise and chi-squared curves almost coincide, indicating that the standardized power of the random noise follows a chi-squared distribution. In Fig. 5(b), the standardized power of the noisy signal does not follow a chi-squared distribution.

In Fig. 5(a), we define:

$$\begin{cases} p(x>c) = \alpha \\ c = \chi_2^2(\alpha) \end{cases}$$
 (18)

where p is the cumulative probability of the chi-squared distribution; α is the confidence level; and c is the denoising threshold value for the standardized power spectrum $P'_{\nu}(k)$,

and the noise components less than c are suppressed. The value of α can be adjusted to improve the denoising performance. For example, more random noise is suppressed at high values of α .



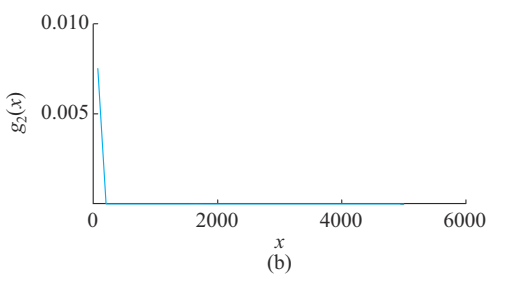


Fig. 5. Probability density curves of chi-squared distribution, random noise, and a noisy signal. (a) Random noise. (b) Noisy signal.

When c is determined, the threshold value must be $c\sigma_V^2$ for the noise power spectrum $P_v(k)$ according to (14). Thus, according to (11), S_{th} in the amplitude spectrum can be set to be:

$$S_{th} = \sigma_V \sqrt{c} \tag{19}$$

However, the random noise of power signals is difficult to obtain. Thus, the standard deviation σ_V is unknown. Therefore, an iterative method for estimating the standard deviation of the noise is proposed.

2) Iterative Method for Threshold Setting

According to the property of the chi-squared distribution, the mean and variance of the standardized noise power are:

$$\begin{cases} E(P_v'(k)) = 2\\ Var(P_v'(k)) = 4 \end{cases}$$
 (20)

As shown in Fig. 5(b), the standardized power of the noisy signal does not follow a chi-squared distribution. Thus, its mean and variance do not satisfy (20). However, some effective frequency components can be removed to ensure that the residual power spectrum has a mean of 2 and a variance of 4. At this time, the standard deviation of the residual spectrum can be considered as σ_V . Based on this concept, the following iterative steps are proposed.

Step 1: obtain the spectrum of the power signals and initialize the iteration index i=0:

$$\begin{cases} R_Y^i(k) = real(Y(k)) \\ I_Y^i(k) = imag(Y(k)) \end{cases}$$
 (21)

where $R_Y^i(k)$ and $I_Y^i(k)$ are the real and imaginary parts of the frequency spectrum of the signal, respectively.

Step 2: standardize the power spectrum:

$$RI_{y}^{i} = [R_{y}^{i}(0) \dots R_{y}^{i}(M-1) I_{y}^{i}(0) \dots I_{y}^{i}(M-1)]$$
 (22)

$$\sigma_Y^i = std(\mathbf{R}\mathbf{I}_Y^i) \tag{23}$$

$$P_{Y}^{i}(k) = \frac{(R_{Y}^{i}(k))^{2} + (I_{Y}^{i}(k))^{2}}{(\sigma_{Y}^{i})^{2}}$$
(24)

where RI_{γ}^{i} is a vector composed of $R_{\gamma}^{i}(k)$ and $I_{\gamma}^{i}(k)$; σ_{γ}^{i} is the standard deviation of RI_{γ}^{i} ; and $P_{\gamma}^{i}(k)$ is the standardized power spectrum.

Step 3: calculate the variance and mean of the i^{th} standardized power spectrum:

$$\begin{cases} \lambda_{Y}^{i} = Var(P_{Y}^{i}(k)) \\ E(P_{Y}^{i}(k)) = 2 \end{cases}$$
 (25)

In each case, the mean of the standardized power spectrum must be 2, as shown in Appendix A Section B. Thus, only the variance is used to determine the standard deviation of the noise.

Step 4: eliminate the maximum power spectrum that represents the effective frequency components:

$$\mathbf{R}_{Y}^{i+1} = \left[R_{Y}^{i}(0) \ R_{Y}^{i}(1) \ \dots \ R_{Y}^{i}(j-1) \ R_{Y}^{i}(j+1) \ \dots \right]$$
 (26)

$$I_{Y}^{i+1} = \left[I_{Y}^{i}(0) \ I_{Y}^{i}(1) \ \dots \ I_{Y}^{i}(j-1) \ I_{Y}^{i}(j+1) \ \dots \right]$$
 (27)

where j is the index of the maximum power spectrum.

Step 5: return to Step 2 to recalculate the variance until it is less than 4, and define the maximum iteration index as i_{max} .

Step 6: find the standard deviation corresponding to the variance closest to 4, and set it as σ_{ν} :

$$i_{v} = \min \left| \lambda_{Y}^{i} - 4 \right| \quad 0 \le i \le i_{\text{max}}$$
 (28)

$$\sigma_V = \sigma_Y^{l_v} \tag{29}$$

where i_{ν} is the index of the variance closest to 4; and min(·) is a function that returns the index of the minimum value in a data sequence.

This method is used to estimate the standard deviation of the noise. Then, the threshold value can be obtained using (19). After multiple tests, most noise can be suppressed to achieve good denoising performance at a confidence level of 0.01. In this paper, $c = \chi_2^2(0.01) = 9.21$ is used.

The proposed denoising method adjusts the threshold value adaptively for different noise levels. Note that the synchrophasor estimation algorithm can filter the OOB interference signals. Therefore, only the random noise in the measurement band (0 to 100 Hz in this paper) needs to be analyzed.

D. Sensitivity to Length of Data Window

The FFT suffers from the spectrum leakage and the fence effect, and its frequency resolution is limited by the length of the data window. These problems may impact the denoising performance. Therefore, it is necessary to analyze the influence of the length of the data window on the performance of the proposed denoising method.

The test signal model is defined in (16). The residual noise after using the proposed denoising method is:

$$v'(k) = y'(k) - x(k)$$
 (30)

The SNR of the denoised signal can be obtained with (17). The noise level is set to be 40 dB. The SNR of denoised signal

for different lengths of the data window is shown in Fig. 6. The noise level decreases as the length of the data window of the FFT increases. However, the growth rate significantly decreases when the length of the data window is greater than 4 s. At this time, any increase in the length of the data window to improve the denoising performance is ineffective because of a substantial increase in the computational burden. Therefore, 4 s is used as the length of the data window in the proposed denoising method. The PMU calibrator only provides high-accuracy measurements for the reference values and has no latency requirements. Thus, a data window of 4 s is acceptable for the PMU calibrator.

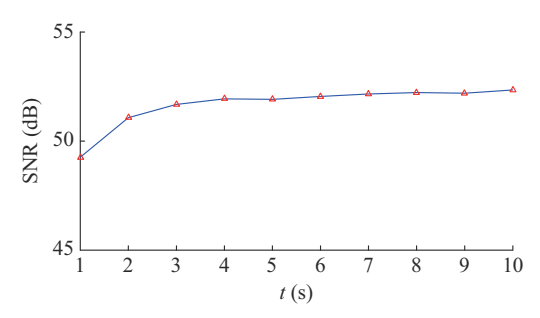


Fig. 6. SNR of denoised signal for different lengths of data window.

The amplitude spectrum of a simulated signal for which the length of the data window is 4 s, is shown in Fig. 7, where the red line represents the threshold value (0.0253 A). Most components are less than 0.0253 A, indicating that most random noise is suppressed.

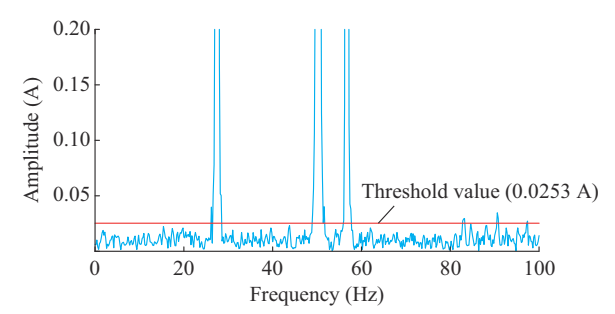


Fig. 7. Magnitude of response of simulated signal and denoising threshold.

The denoised signal still contains approximately 52 dB of noise in the measurement band, indicating the limits to the denoising ability of the proposed denoising method. The reason is that the noise spectrum is continuous, whereas the proposed FFT-based method can only deal with noise components at discrete frequency points. Owing to the fence effect, the noise between two frequency points cannot be suppressed. However, the proposed denoising method can still significantly improve the synchrophasor accuracy under static and dynamic conditions, as discussed in the next section.

V. PERFORMANCE VERIFICATION

A. Synchrophasor Estimation Method

In this paper, the reporting rate F_r is 50 Hz, and the sampling frequency is 1200 Hz. A PMU calibrator is developed,

and its hardware composition is described in [9]. The proposed synchrophasor algorithm is implemented using a PMU calibrator. In addition, it is necessary to analyze the hardware performance and memory capacity requirements to record the waveforms. In the PMU calibrator, a common format for transient data exchange (COMTRADE) file is used to record the three-phase voltage and current waveforms. Since only the fundamental measurement is considered, the sampling frequency does not need to be too high. One minute of waveform data is stored in a file. From experimental tests, the size of one file is approximately 1.8 MB. In general, it is sufficient for the PMU calibrator to store the waveform files for one day. Thus, the required storage capacity is $60 \times 24 \times 1.8 = 2592 \text{ MB} \approx 2.6 \text{ GB}$. Because recording the waveforms does not involve complex algorithms, it has a low computational complexity. Compared with phasor measurement and denoising methods, the impact of the recorded waveforms on the hardware performance can be ignored.

A high-precision generator is used to test the PMU calibrator according to the test conditions specified in an IEEE standard [7]. In addition, the calibrator method in [27] (denoted as PA) and a novel synchrophasor method in [37] (denoted as PB), are used for comparison to illustrate the advantages of the proposed synchrophasor algorithm. Compared with other calibrator algorithms, PA is a universal calibrator algorithm and is not related to signal models. Thus, it can be used for field PMU test. PB is a synchrophasor estimation method with good performance under static and dynamic conditions. Therefore, these two methods are selected for comparison. PA uses a quadratic expansion to approach the dynamic amplitude and phase in the observation interval. Then, the fitting coefficients are solved using the leastsquares (LS) method. PB designs an optimized cosine selfconvolution window and combines it with an interpolated DFT to estimate the synchrophasor.

The test results are listed in Tables II, III, and IV. The Chinese PMU standard (CHS) is also listed to verify the performance of the proposed denoising method [38]. The CHS uses the amplitude and phase errors to evaluate the phasor accuracy. Thus, the equivalent TVE is listed in Table II.

TABLE II
THE MAXIMUM SYNCHROPHASOR ERRORS FOR STANDARD TEST

T4 4	TVE (%)					
Test type	IEEE	CHS	Proposed	PA	PB	
Off-nominal	1.0	0.425	0.0053	0.067	0.003	
Harmonic	1.0	0.852	0.0024	0.033	0.212	
OOB	1.3	1.853	0.0074	0.068	0.062	
AM	3.0	0.578	0.0036	0.009	0.407	
PM	3.0	0.907	0.0076	0.011	0.369	
Frequency ramp	1.0	0.907	0.0050	0.049	0.016	

The estimation accuracy of PA is 10 times higher than the IEEE standard requirements. However, the ROCOF accuracy is only approximately two times higher than that of the CHS in off-nominal tests. Thus, PA cannot be applied to PMU test in China. The accuracy of PB is poor. In particular, the

frequency errors exceed the limitations of harmonic and OOB test. The proposed method has higher accuracy than that of PA. The synchrophasor, frequency, and ROCOF accuracies are at least two orders of magnitude higher than the standard requirements under static and dynamic conditions. For the harmonic and OOB test, the designed complex bandpass filter can filter the interference signals successfully, and the frequency and ROCOF are estimated accurately. Therefore, the developed PMU calibrator has good estimation performance for PMU test.

TABLE III
THE MAXIMUM FREQUENCY ERRORS FOR STANDARD TEST

Test trans	Frequency error (Hz)					
Test type	IEEE	CHS	Proposed	PA	PB	
Off-nominal	0.005	0.002	1.1×10 ⁻⁵	5.0×10 ⁻⁵	0.002	
Harmonic	0.025	0.004	8.0×10^{-6}	1.9×10^{-4}	0.075	
OOB	0.010	0.025	1.9×10^{-5}	2.6×10^{-3}	0.027	
AM	0.300	0.025	8.0×10^{-6}	1.9×10^{-4}	0.039	
PM	0.300	0.300	9.1×10^{-5}	8.5×10^{-3}	0.024	
Frequency ramp	0.010	0.010	1.9×10^{-5}	3.1×10^{-4}	0.007	

Toot true	RFE (Hz/s)					
Test type	IEEE	CHS	Proposed	PA	PB	
Off-nominal	0.1	0.01	8.9×10 ⁻⁵	0.0046	0.012	
Harmonic		0.02	7.0×10^{-5}	0.0040	0.218	
OOB			2.8×10^{-4}	0.2540	1.632	
AM	14.0	0.10	6.7×10^{-5}	0.0110	0.925	
PM	14.0	3.00	4.8×10^{-3}	0.5220	1.431	
Frequency ramp	0.2	0.20	8.3×10^{-4}	0.0160	0.013	

B. Denoising Method

The denoising method may be used to suppress the random noise in scenarios B and C, as shown in Fig. 1. Denoising methods based on the wavelet transform (DB) [29] and SVD (DC) [31] are compared to verify the advantages of the proposed method (DA).

The simulation signal is presented in (31) and the random noise of 30 dB is added.

$$y(t) = 50 \sqrt{2} \left[1 + 0.2\cos(2\pi \times 15t)\right]\cos(2\pi \times 50t) + noise$$
 (31)

The DB and DC methods are used to denoise the amplitude modulation signal, and the magnitudes of responses of original and denoised signals for DB and DC methods are shown in Fig. 8. The DB method is similar to a low-pass filter. Thus, it cannot suppress the random noise in the low-frequency band, although it has good high-frequency noise suppression capability. The DC method has better suppression performance for low-frequency noise because the dominant components can be obtained by SVD. However, the noise near the frequency components is difficult to suppress.

The magnitudes of responses of original and denoised signals for DA method are shown in Fig. 9. Most of the noise has been removed, including that in the low-frequency band.

The noise between the two frequency components can also be suppressed. Thus, DA is suitable for dynamic signal denoising. DA has better denoising performance than that of DB and DC methods. However, some noises may remain in the denoised signals because it is difficult to distinguish the random noise from the frequency components completely with the threshold value.

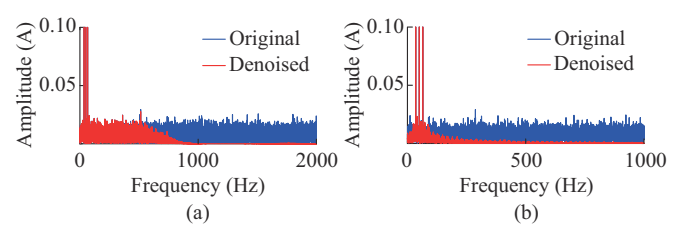


Fig. 8. Magnitudes of responses of original and denoised signals for DB and DC methods. (a) DB method. (b) DC method.

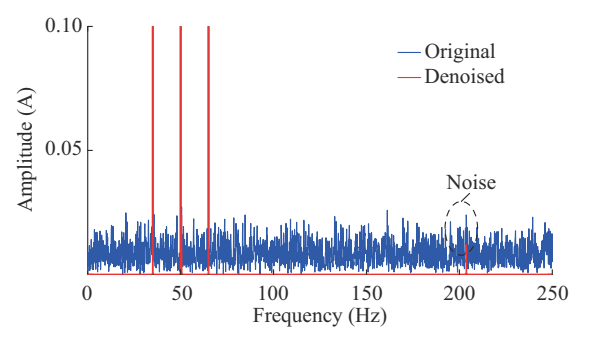


Fig. 9. Magnitudes of responses of original and denoised signals for DA method.

C. Phasor Accuracy of Denoised Signals

After analyzing the field-recorded data, the field current signals may still contain the random noise of up to 30 dB. Thus, 30 dB of noise is added to the static and dynamic signals. The maximum synchrophasor errors of different denoising methods are listed in Table V. The noise test is not specified in the existing PMU standards. Therefore, there are no standard requirements as evaluation indicators for noise test. In addition, the frequency and ROCOF of the current signals need not be estimated. Therefore, they are not provided in Table V.

TABLE V
THE MAXIMUM SYNCHROPHASOR ERRORS OF DIFFERENT DENOISING
METHODS FOR CURRENT SIGNALS WITH 30 DB OF NOISE

Toot true	TVE (%)				
Test type	Noise	DA	DB	DC	
Off-nominal	1.761	0.668	1.763	0.841	
AM	1.792	0.705	1.792	1.332	
PM	1.782	0.681	1.781	1.392	
Frequency ramp	1.793	0.792	1.793	1.348	

The synchrophasor errors of the noisy signals are relatively large. DB cannot suppress the random noise in the low-frequency band, which leads to unchanged synchrophasor errors. DC can remove the noise from the static signals but has poor denoising performance for dynamic signals. For

DA, the synchrophasor errors of the denoised signals are less than half of the signals without denoising. Therefore, the proposed method has better denoising performance than DB and DC methods.

The analysis of the field-recorded data shows that the SNR of the field voltage signals is as high as 50 dB. Thus, 50 dB of noise is added to the test signals. The results are shown in Tables VI and VII. Because DB could not suppress the noise, it is not included in Tables VI and VII. Similar to the results in Table V, DC has a good denoising effect for static signals but not for dynamic signals. The synchrophasor accuracy of the proposed method under static and dynamic conditions is improved by approximately 50%, except for the frequency ramp test. The fundamental frequency linearly changes over time during frequency ramp test. Thus, there is significant spectrum leakage, resulting in low denoising performance. The frequency accuracy is improved by 3-6 times, and the ROCOF accuracy is improved by 4-10 times compared with that of noisy signals. Therefore, the proposed denoising method provides better denoising performance and higher estimation accuracy than the other methods.

TABLE VI
THE MAXIMUM SYNCHROPHASOR ERRORS OF DIFFERENT DENOISING
METHODS FOR VOLTAGE SIGNALS WITH 50 DB OF NOISE

Test type		TVE (%)	
	Noise	DA	DC
Off-nominal	0.173	0.083	0.086
AM	0.179	0.053	0.133
PM	0.177	0.069	0.154
Frequency ramp	0.180	0.108	0.182

TABLE VII
THE MAXIMUM FREQUENCY AND ROCOF ERRORS OF DIFFERENT
DENOISING METHODS FOR VOLTAGE SIGNALS WITH 50 DB OF NOISE

T4 4	FE (Hz)			RFE (Hz/s)		
Test type	Noise	DA	DC	Noise	DA	DC
Off-nominal	0.012	0.002	0.003	0.708	0.064	0.112
AM	0.012	0.002	0.007	0.735	0.122	0.328
PM	0.018	0.004	0.011	1.102	0.232	0.671
Frequency ramp	0.012	0.004	0.011	0.784	0.187	0.782

VI. CONCLUSION

In this paper, a general test and calibration framework are proposed for field PMU test in different scenarios. The framework comprises a PMU calibrator and an analysis center. The main focus of Part I is on the algorithms for the PMU calibrator. A general design method based on a complex bandpass filter is developed for accurate synchrophasor estimation in multiple scenarios. A Fourier-transform-based threshold denoising method is proposed to improve the antinoise capability of the PMU calibrator. The threshold value is determined iteratively according to the frequency-domain chi-squared distribution of the random noise. Simulation and experimental test results show that the PMU calibrator has a higher accuracy than that of other calibrator algorithms and

denoising methods for complex field signals. The accuracy of the synchrophasor estimation method is 100 times higher than the standard requirements. The proposed denoising method can double the phasor accuracy and triple the frequency and ROCOF accuracy under noisy conditions. Thus, the method can provide reference values for error analysis of field PMUs. The analysis center and applications of the proposed test method are presented in Part II.

APPENDIX A

A. Frequency and ROCOF Estimation Method

In [9], a frequency and ROCOF estimation method based on the filtering characteristics of the LS method is proposed. As the frequency and ROCOF have the same solution processes, ROCOF estimation is provided as an example.

The second-order polynomial is used to approximate the time-varying frequency in the observation window:

$$f(t) = d_0 + d_1 t + d_2 t^2 \tag{A1}$$

where d_0 , d_1 , and d_2 are the polynomial coefficients that can be obtained by the LS method:

$$\boldsymbol{D} = (\boldsymbol{P}_{f}^{T} \boldsymbol{P}_{f})^{-1} \boldsymbol{P}_{f}^{T} \boldsymbol{F}$$
 (A2)

where F consists of M+1 adjacent measured frequencies (M is an even number); D is composed of the polynomial coefficients ($D = [d_0, d_1, d_2]^T$); and P_f is related to F_c and M (F_c is the calculation rate of the synchrophasor).

By deriving (A1) and setting the time tag at the center of the observation window, the ROCOF can be calculated as d_1 .

The above method can estimate the ROCOF accurately in the static state but will cause larger errors when the oscillation exists in the power system. To this end, an improved method is proposed.

The frequency and ROCOF of power oscillation can be expressed as:

$$f(t) = f_0 - a_{\rm m} \sin(2\pi f_{\rm m} t + \varphi_{\rm p}) \tag{A3}$$

$$rf(t) = -b_{\rm m} a_{\rm m} \cos(2\pi f_{\rm m} t + \varphi_{\rm n}) \tag{A4}$$

where $a_{\rm m} = -f_{\rm m}k_{\rm p}$; $b_{\rm m} = 2\pi f_{\rm m}$; and $f_{\rm m}$, $k_{\rm p}$, and $\varphi_{\rm p}$ are the modulation frequency, depth, and initial phase, respectively.

In (A2), let

$$\mathbf{Q}_{f} = (\mathbf{P}_{f}^{T} \mathbf{P}_{f})^{-1} \mathbf{P}_{f}^{T} = \begin{bmatrix} q_{00} & q_{01} & \cdots & q_{0M} \\ q_{10} & q_{11} & \cdots & q_{1M} \\ q_{20} & q_{21} & \cdots & q_{2M} \end{bmatrix} = \begin{bmatrix} \mathbf{q}_{0} \\ \mathbf{q}_{1} \\ \mathbf{q}_{2} \end{bmatrix}$$
(A5)

Once F_c and M are determined, P_f and Q_f can be calculated offline. As the ROCOF is equal to d_1 in the observation window, its estimation equation can be rewritten as:

$$r\hat{f}(k) = \sum_{i=0}^{M} q_{1i} f(k - M/2 + i)$$
 (A6)

Equation (A6) is equivalent to using an M^{th} -order filter $q_1 = [q_{10}, q_{11}, ..., q_{1M}]$ to filter the measured frequencies f(k).

According to the properties of an FIR filter, the estimated ROCOF with the time is:

$$\hat{r}f(t) = -\left|Q_1(f_{\rm m})\right| a_{\rm m}\cos(2\pi f_{\rm m}t + \varphi_{\rm p}) \tag{A7}$$

where $\left|Q_{1}(f_{\mathrm{m}})\right|$ is the amplitude-frequency characteristic of q_{1} .

Then, the measurement errors in the ROCOF can be expressed as:

$$e_{\rm rf}(t) = rf(t) - \hat{r}f(t) = -\left(\frac{b_{\rm m}}{|Q_1(f_{\rm m})|} - 1\right) |Q_1(f_{\rm m})| a_{\rm m}\cos(2\pi f_{\rm m}t + \varphi_{\rm p}) \quad (A8)$$

The errors are related to the modulation frequency $f_{\rm m}$. If $e_{\rm rf}(t)$ can be obtained, the errors in the ROCOF may be eliminated

According to the spectral characteristics of q_2 and the properties of an FIR filter, the expression for the second derivative in the time domain is:

$$c_2(t) = -|Q_2(f_m)||Q_1(f_m)|a_m\cos(2\pi f_m t + \varphi_p)$$
 (A9)

where $|Q_2(f_m)|$ is the amplitude-frequency characteristic of q_2 . Substituting (A9) into (A8), the measurement error in the RO-COF is

$$e_{\rm rf}(t) = \left(\frac{b_{\rm m}}{|Q_1(f_{\rm m})|} - 1\right) \frac{c_2(t)}{|Q_2(f_{\rm m})|}$$
 (A10)

Let

$$K_{2} = \left(\frac{b_{\rm m}}{|Q_{1}(f_{\rm m})|} - 1\right) \frac{1}{|Q_{2}(f_{\rm m})|} \tag{A11}$$

The change in K_2 with the modulation frequency is very small with a difference of 8×10^{-7} . Therefore, K_2 can be considered as a constant independent of the modulation frequency (the constant is 2.85×10^{-5} in this paper). The measurement error can be eliminated as:

$$r\hat{f}_{c}(k) = r\hat{f}(k) - 2.85 \times 10^{-5} c_{2}(k)$$
 (A12)

where $r\hat{f}_{c}(k)$ is the final estimated ROCOF.

B. Mean of Standardized Power Spectrum

The real and imaginary parts of the signal spectrum are denoted as R(k) and I(k), respectively $(0 \le k \le N-1)$. They comprise a vector:

$$RI = [R(0) \ R(1) \ \dots \ R(N-1) \ I(0) \ I(1) \ \dots \ I(N-1)]$$
 (A13)

The mean and variance of **RI** can be obtained by:

$$\mu = \frac{\sum_{k=0}^{2N-1} RI(k)}{2N} = \frac{\sum_{k=0}^{N-1} (R(k) + I(k))}{2N}$$
(A14)

$$\sigma^{2} = \frac{\sum_{k=0}^{2N-1} (RI(k) - \mu)^{2}}{2N} = \frac{\sum_{k=0}^{N-1} \left[(R(k) - \mu)^{2} + (I(k) - \mu)^{2} \right]}{2N} = \frac{\sum_{k=0}^{N-1} \left[(R(k)^{2} + I(k)^{2}) - 2\mu(R(k) + I(k)) + 2\mu^{2} \right]}{2N} = \frac{\sum_{k=0}^{N-1} (R(k)^{2} + I(k)^{2})}{2N} - 2\mu \frac{\sum_{k=0}^{N-1} (R(k) + I(k))}{2N} + 2\mu^{2} = \frac{\sum_{k=0}^{N-1} (R(k)^{2} + I(k)^{2})}{2N}$$
(A15)

The standardized power spectrum is:

$$P'(k) = \frac{R(k)^2 + I(k)^2}{\sigma^2}$$
 (A16)

The mean of the above power spectrum is:

$$\mu_{P} = \frac{\sum_{k=0}^{N-1} P'(k)}{N} = \frac{\sum_{k=0}^{N-1} (R(k)^{2} + I(k)^{2})}{N\sigma^{2}}$$
(A17)

By substituting (A15) into (A17), $\mu_P = 2$. Therefore, the mean of the standardized power spectrum must be 2 in every case.

REFERENCES

- A. Gphadke, T. Bi, and V. Tech, "Phasor measurement units, WAMS, and their applications in protection and control of power systems," *Journal of Modern Power Systems and Clean Energy*, vol. 6, no. 4, pp. 619-629, Apr. 2018.
- [2] P. Risbud, N. Gatsis, and A. Taha, "Multi-period power system state estimation with PMUs under gps spoofing attacks," *Journal of Mod*ern Power Systems and Clean Energy, vol. 8, no. 4, pp. 597-606, Jul. 2020.
- [3] M. U. Usman and M. O. Faruque, "Applications of synchrophasor technologies in power systems," *Journal of Modern Power Systems and Clean Energy*, vol. 7, no. 2, pp. 211-226, Mar. 2019.
- [4] P. Rajaraman, N. A. Sundaravaradan, B. Mallikarjuna et al., "Robust fault analysis in transmission lines using Synchrophasor measurements," Protection and Control of Modern Power Systems, vol. 3, no. 14, pp. 1-13, Apr. 2018.
- [5] W. Fan and Y. Liao, "Wide area measurements based fault detection and location method for transmission lines," *Protection and Control of Modern Power Systems*, vol. 4, no. 7, pp. 1-12, Mar. 2019.
- [6] J. P. Desai and V. H. Makwana, "Phasor measurement unit incorporated adaptive out-of-step protection of synchronous generator," *Journal of Modern Power Systems and Clean Energy*, vol. 9, no. 5, pp. 1032-1042, Sept. 2021.
- [7] Measuring Relays and Protection Equipment—Part 118-1: Synchrophasor for Power Systems—Measurements, IEC/IEEE Standard 60255-118-1, 2018.
- [8] Z. Jin, H. Zhang, F. Shi et al., "A robust and adaptive detection scheme for interharmonics in active distribution network," *IEEE Trans*actions on Power Delivery, vol. 33, no. 5, pp. 2524-2534, Oct. 2018.
- [9] S. Xu, H. Liu, T. Bi et al., "A high-accuracy phasor estimation algorithm for PMU calibration and its hardware implementation," IEEE Transactions on Smart Grid, vol. 11, no. 4, pp. 3372-3383, Jul. 2020.
- [10] F. L. Grando, A. E. Lazzaretti, G. W. Denardin et al., "A synchrophasor test platform for development and assessment of phasor measurement units," *IEEE Transactions on Industry Applications*, vol. 54, no. 4, pp. 3122-3131, Jul. 2018.
- [11] R. Ghiga, K. Martin, Q. Wu et al., "Phasor measurement unit test under interference conditions," *IEEE Transactions on Power Delivery*, vol. 33, no. 2, pp. 630-639, Apr. 2018.
- [12] H. Liu, T. Bi, and Q. Yang, "The evaluation of phasor measurement units and their dynamic behavior analysis," *IEEE Transactions on In*strumentation and Measurement, vol. 62, no. 6, pp. 1479-1485, Jun. 2013.
- [13] G. Frigo, D. Colangelo, A. Derviškadić et al., "Definition of accurate reference synchrophasors for static and dynamic characterization of PMUs," *IEEE Transactions on Instrumentation and Measurement*, vol. 66, no. 9, pp. 2233-2246, Sept. 2017.
- [14] C. Qian and M. Kezunovic, "Synchrophasor reference algorithm for PMU calibration system," in *Proceedings of 2016 IEEE/PES Transmis*sion and Distribution Conference and Exposition (T&D), Dallas, USA, Jul. 2016, pp. 1-5.
- [15] Y. Tang, G. N. Stenbakken, and A. Goldstein, "Calibration of phasor measurement unit at NIST," *IEEE Transactions on Instrumentation* and Measurement, vol. 62, no. 6, pp. 1417-1422, Jun. 2013.
- [16] C. Qin, J. Greig-Prine, Z. Nie et al., "Remote PMU testing using low-cost FPGA platform and PPA following IEEE TSS," in Proceedings of 2019 IEEE Industry Applications Society Annual Meeting, Baltimore, USA, Aug. 2019, pp. 1-7.
- [17] D. Georgakopoulos and S. Quigg, "Precision measurement system for the calibration of phasor measurement units," *IEEE Transactions on*

- Instrumentation and Measurement, vol. 66, no. 6, pp. 1441-1445, Jun. 2017
- [18] T. Becejac and P. Dehghanian, "PMU multilevel end-to-end testing to assess synchrophasor measurements during faults," *IEEE Power and Energy Technology Systems Journal*, vol. 6, no. 1, pp. 71-80, Mar. 2019
- [19] D. Slomovitz, D. Izquierdo, L. Trigo et al., "Online verification system for phasor measurement units," in *Proceedings of 2020 Conference on Precision Electromagnetic Measurements (CPEM)*, Denver, USA, Jul. 2020, pp. 1-2.
- [20] J. A. de la O. Serna, M. R. A. Paternina, and A. Zamora-Mendez, "Assessing synchrophasor estimates of an event captured by a phasor measurement unit," *IEEE Transactions on Power Delivery*, vol. 36, no. 5, pp. 3109-3117, Oct. 2021.
- [21] S. Nanda and P. K. Dash, "A Gauss-Newton ADALINE for dynamic phasor estimation of power signals and its FPGA implementation," *IEEE Transactions on Instrumentation and Measurement*, vol. 67, no. 1, pp. 45-56, Jan. 2018.
- [22] C. Huang, X. Xie, and H. Jiang, "Dynamic phasor estimation through DSTKF under transient conditions," *IEEE Transactions on Instrumen*tation and Measurement, vol. 66, no. 11, pp. 2929-2936, Nov. 2017.
- [23] P. Romano and M. Paolone, "Enhanced interpolated-DFT for synchrophasor estimation in fpgas: theory, implementation, and validation of a PMU prototype," *IEEE Transactions on Instrumentation and Measure*ment, vol. 63, no. 12, pp. 2824-2836, Dec. 2014.
- [24] A. Derviškadić, P. Romano, and M. Paolone, "Iterative-interpolated DFT for synchrophasor estimation: a single algorithm for P- and Mclass compliant PMUs," *IEEE Transactions on Instrumentation and Measurement*, vol. 67, no. 3, pp. 547-558, Mar. 2018.
- [25] M. A. Platas-Garza and J. A. de la O. Serna, "Dynamic phasor and frequency estimates through maximally flat differentiators," *IEEE Transactions on Instrumentation and Measurement*, vol. 59, no. 7, pp. 1803-1811, Jul. 2010.
- [26] J. R. Razo-Hernandez, A. Mejia-Barron, D. Granados-Lieberman et al., "A new phasor estimator for PMU applications: P class and M class," *Journal of Modern Power Systems and Clean Energy*, vol. 8, no. 1, pp. 55-66, Jan. 2020.
- [27] J. Ren and M. Kezunovic, "An adaptive phasor estimator for power system waveforms containing transients," *IEEE Transactions on Pow*er Delivery, vol. 27, no. 2, pp. 735-745, Apr. 2012.
- er Delivery, vol. 27, no. 2, pp. 735-745, Apr. 2012.

 [28] H. Touati and K. Khaldi, "Speech denoising by adaptive filter LMS in the EMD framework," in Proceedings of 2018 15th International Multi-Conference on Systems, Signals & Devices (SSD), Yasmine Hammamet, Tunisia, Jan. 2018, pp. 1-4.
- [29] J. Tang, S. Zhou, and C. Pan, "A denoising algorithm for partial discharge measurement based on the combination of wavelet threshold and total variation theory," *IEEE Transactions on Instrumentation and Measurement*, vol. 69, no. 6, pp. 3428-3441, Jun. 2020.
- [30] S. Shukla, S. Mishra, and B. Singh, "Power quality event classification under noisy conditions using EMD-based de-noising techniques," *IEEE Transactions on Industrial Informatics*, vol. 10, no. 2, pp. 1044-1054, May 2014.
- [31] S. Govindarajan, J. Subbaiah, A. Cavallini et al., "Partial discharge random noise removal using hankel matrix-based fast singular value decomposition," *IEEE Transactions on Instrumentation and Measure*ment, vol. 69, no. 7, pp. 4093-4102, Jul. 2020.
- [32] M. Narasimhappa, S. L. Sabat, and J. Nayak, "Fiber-optic gyroscope signal denoising using an adaptive robust Kalman filter," *IEEE Sen*sors Journal, vol. 16, no. 10, pp. 3711-3718, May 2016.
- [33] P. L. Shui, "Image denoising algorithm via doubly local Wiener filtering with directional windows in wavelet domain," *IEEE Signal Processing Letter*, vol. 12, no. 10, pp. 681-684, Oct. 2005.
- [34] S. Xu, H. Liu, and T. Bi, "Field PMU test and calibration method—part II: test signal identification methods and field test applications," *Journal of Modern Power Systems and Clean Energy*, doi: 10.35833/MPCE.2021.000527
- [35] S. Xu, H. Liu, and T. Bi, "A general design method for phasor estimation in different applications," *IEEE Transactions on Smart Grid*, vol. 12 no. 3, pp. 2307-2319, May 2021.
- [36] R. Li, M. Kang, and G. Wang, "Evaluation of statistic probability distribution functions: II. Chi-squared probability function and the inverse functions of z, t, F, and Chi-squared distributions," in Proceedings of 2016 International Conference on Computational Science and Computational Intelligence (CSCI), Las Vegas, USA, Sept. 2016, pp. 1253-1260.
- [37] T. Jin and W. Zhang, "A novel interpolated DFT synchrophasor estimation algorithm with an optimized combined cosine self-convolution

- window," *IEEE Transactions on Instrumentation and Measurement*, vol. 70, pp. 1-10, Jan. 2021.
- [38] Technology Specifications of Power System Real Time Dynamic Monitoring System, State Grid Corporation of China Standard Q/GDW 1131-2014, 2015.

Sudi Xu is currently pursuing the Ph.D. degree in electrical engineering at North China Electric Power University, Beijing, China. His research interests include synchrophasor estimation and phasor measurement unit calibration.

Hao Liu received the Ph.D. degree in electrical engineering from North China Electric Power University, Beijing, China in 2015. He is currently an Associate Professor with North China Electric Power University. His research interests include synchronized measurement, testing and calibration and its applications.

Tianshu Bi received the Ph.D. degree in electrical and electronic engineering from the University of Hong Kong, Hong Kong, China, in 2002. She is currently a Professor at North China Electric Power University, Beijing, China. Her research interests include power system protection and control, and synchrophasor measurement and its applications.